Targeted MRI for Breast Cancer using Iron Oxide Nanoparticles

Introduction

Magnetic Resonance Imaging (MRI) utilizes a powerful magnetic field to align the nuclear magnetization of hydrogen atoms in water in the body without the use of ionizing radiation. Iron oxide (IO) nanoparticles are the only FDA approved nanoparticles used as a MRI contrast agent. Paramagnetic IO nanoparticles can induce remarkably strong magnetic resonance imaging contrast and have a large surface area and versatile surface chemistry for the introduction of biomolecules. Here we present uPA receptor-targeted ATF-IO nanoparticles as molecularly targeted, dual modality imaging agents for in vivo imaging of breast cancer.

Materials:

Ocean's iron oxide particle SHP10 (-COOH surface groups, 10 nm in size), conjugation kit (ICK-10), recombinant ATF (amino-terminal fragment of the high affinity receptor binding domain of urokinase-type plasminogen activator (uPA)); mouse mammary carcinoma cell line 4T1; human breast cancer cell line T47D.

Procedures:

1. **Conjugation of ATF to IO particles:** Conjugate ATF to SHP10 using ICK kit according to the instruction. The SHP to ATF molar ratio was 1:20. The conjugates were purified by a spin column with molecular weight cutoff of 100K (Pall Corp.)
2. ***In vitro* tumor cell MRI imaging:** Cells were incubated with serum-free medium containing 13.5 pmole nontargeted IO or ATF-IO nanoparticles at 37°C for 3 hr. After washing with PBS, the cells were embedded in 0.8% agarose in 24-well plates. Plates were then scanned in a 3-T MRI scanner (Philips Medical System) using a T_1-weighted gradient echo sequence and a multi-echo T_2-weighted fast spin echo sequence, which simultaneously collects a series of data points at different echo times (i.e., 20 echo time (TE) points from 10-200 ms with a 10 ms interval) for T_2 relaxometry measurement.
3. **Establishment of s.c. mice tumor model:** 4T1 cells were injected s.c. into the back flank area of 6- to 8- wk-old female BALB/c or nude mice.
4. **Establishment of intraperitoneal (i.p.) metastatic mammary tumore model:** 4T1 cells stably transfected with a firefly luciferase gene were directly injected into the upper right side of the peritoneal cavity. Tumor growth was monitored by bioluminescence imaging using the Xenogen bioluminescence imaging system (Xenogen Corp.)
5. **In vivo MRI of mammary tumor lesions:** For precontrast scan, tumor-bearing mice were examined using a 3-T MRI scanner (Philips Medical System), with a customized rodent coil to obtain MRI images. Animals were anesthetized by i.p. injection of a ketamine-xylazine mixture (95:5 mg/kg). Animals were kept warm in the scanner using warm pads. A set of survey images was obtained using T_2-

weighted fast spin echo imaging sequence with repetition time (TR) of 5,000 ms and TE of 120 ms. This was followed by high resolution imaging in the coronal view (i.e., slices cut through from head to tail), with a field of view of 110 x 40 mm, imaging matrix of 256 x 192 (reconstructed to 356 x 256), and 40 slices with 1.1-mm slice thickness without slice gap.

The imaging sequences included T_1- and T_2-weighted spin echo or gradient echo methods and the three-dimensional fast-spoiled gradient echo technique. A TE of 10 ms and TR of 350 ms were used for T_1-weighted spin echo imaging, and TE of 50 ms and TR of 1,500 ms were used for T_2-weighted fast spin echo imaging. A multi-echo T_2 weighted fast spin echo sequence with 12 TEs (range, 10-120 ms; a 10 ms interval) was used to obtain T_2 maps of the whole mouse.

The mice were injected with various nanoparticles suspended in PBS, through the tail vein and then scanned at different time points. For postcontrast scan, care was taken to maintain the same animal positions and use dame imaging sequences and parameters across different scan sessions. Images from pre- and postcontrast administration were compared to evaluate the efficacy of contrast enhancement. Multi-echo T_2 images of slices were used for calculating T_2 maps using a home-developed program based on Matlab (The Mathworks, Inc.). Because IO nanoparticles typically induced T_2-wighted contrast change, the signal reduction in T_2-weighted imaging and change in the T_2 value were used to follow and estimate the accumulation of nontargeted or targeted IO nanoparticles in the area. Region of interest analysis was used to evaluate and quantify the contrast agent-induced changes in MRI signal or T_2 value in the rumor and other selected tissues and organs. Regions of interest of tumors were drawn based on the tumor T_2-signal enhancement in T_2-weighted images or at a long TE time point (TE, 80 ms) in multi-TE T_2-mapping imaging.

Results and Discussions

Binding and internalization of ATF-IO nanoparticles in tumor cells and MRI contrast effect

Prussian blue staining detected a high level of IO nanoparticles in 4T1 cells incubated with ATF-IO but not with nontargeted IO nanoparticles. uPA receptor-negative T47D cells showed only a very low level of nonspecific uptake (Fig. 1A). 4T1 cells incubated with ATF-IO nanoparticles showed MRI contrast with signal reduction in T_2-weighted gradient echo imaging (Fig. 1B, top). T_2 relaxometry measurements indicated that the T_2 value of 4T1 cells bound with ATF-IO nanoparticles dropped significantly compared with those of the T47D cells incubated with ATF-IO nanoparticles and the samples treated with nontargeted IO nanoparticles (Fig. 1B, bottom). Because the T_2 value is a function of the iron concentration, the T_2 relaxometry data suggest that reduction of T_2 relaxation time and MRI signal in T_2 weighted imaging are induced by the specific binding of ATF-IO nanoparticles to the uPA receptor-expression 4T1 cells.

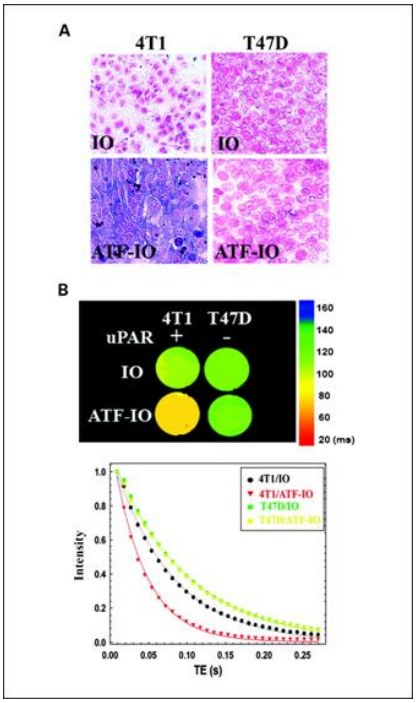

Fig. 1. ATF-IO nanoparticle–induced MRI signal change after binding to tumor cells. A, Prussian blue staining shows specific binding and internalization of ATF-IO nanoparticles in 4T1 cells. A low level of scattered blue staining is found in 4T1 cells incubated with nontargeted iron oxide nanoparticles or urokinase plasminogen activator receptor–negative T47D cells incubated with either IO or ATF-IO nanoparticles. B, reduction of T_2 values in 4T1 cells (top) but not in T47D cells measured by MRI T_2 relaxometry implies the specific binding of ATF-IO nanoparticles to urokinase plasminogen activator receptor–expressing cells. A low T_2 value (orange-to-red color) correlates with a high iron concentration. The fastest T_2 value drop was detected in 4T1 cells incubated with ATF-IO nanoparticles (bottom, red curve). Scale bar, echo time (TE) in milliseconds. T_2 values of each sample/well were calculated from multi-echo images by fitting the decay curve on a pixel-by-pixel basis using the nonlinear mono-exponential algorithm of $M_i = M_0 * \exp(-TEi/T_2)$. M_i is the intensity or magnitude of the measurement at a time point of i. M_0 is the intensity or magnitude of the measurement at the time of zero.

In vivo *targeting and MRI of s.c. mammary tumors in mice*

In BALA/c mice bearing s.c. mouse mammary tumors derived from the 4T1 tumor cell line, T_2-weighted gradient echo imaging and multi-echo fast spin echo imaging showed that ATF-IO nanoparticles selectively accumulated in tumors, as evidenced by a reduction in T_2 values and signal decrease in T_2-weighted images in various areas of the tumor mass (Fig. 2A). The region of interest analysis of MRI signal change showed a 3-fold signal reduction in animals receiving ATF-IO nanoparticles when compared with that in mice receiving nontargeted IO nanoparticles (Fig. 2B). Although we observed decreases in MRI signals in the liver and spleen in the mice injected with ATF-IO nanoparticles because of an iron oxide particle–induced T_2 effect, the reduction in MRI signal was 50% (liver) to 80% (spleen) less than that in mice that received nontargeted iron oxide nanoparticles, suggesting that liver and spleen uptake of the nanoparticles was reduced for ATF-IO nanoparticles (Fig. 2B). To further confirm the distribution of nontargeted and ATF-IO nanoparticles in normal and tumor tissues, Prussian blue staining was done on tissue sections obtained from the mice that received control iron oxide or ATF-IO nanoparticles. Prussian blue–stained cells were detected in the tumor sections of animals that received ATF-IO nanoparticles but not in sections from animals that received nontargeted iron oxide nanoparticles. High magnification images showed the intracellular localization of iron oxide nanoparticles in the cells (Fig. 2C). In normal tissues, we found high levels of Prussian blue–positive cells in the liver and spleen of the mice that received nontargeted iron oxide nanoparticles. However, liver and spleen tissue sections from the group receiving ATF-IO nanoparticles had fewer positive cells. We did not detect iron oxide nanoparticles in the tissue sections of the brain or heart from mice injected with either nontargeted iron oxide or ATF-IO nanoparticles (Fig. 2C). For both groups, the lung and kidney tissues were also negative in most cases (Fig. 2C) and only a few scattered iron-positive cells were detected in some sections.

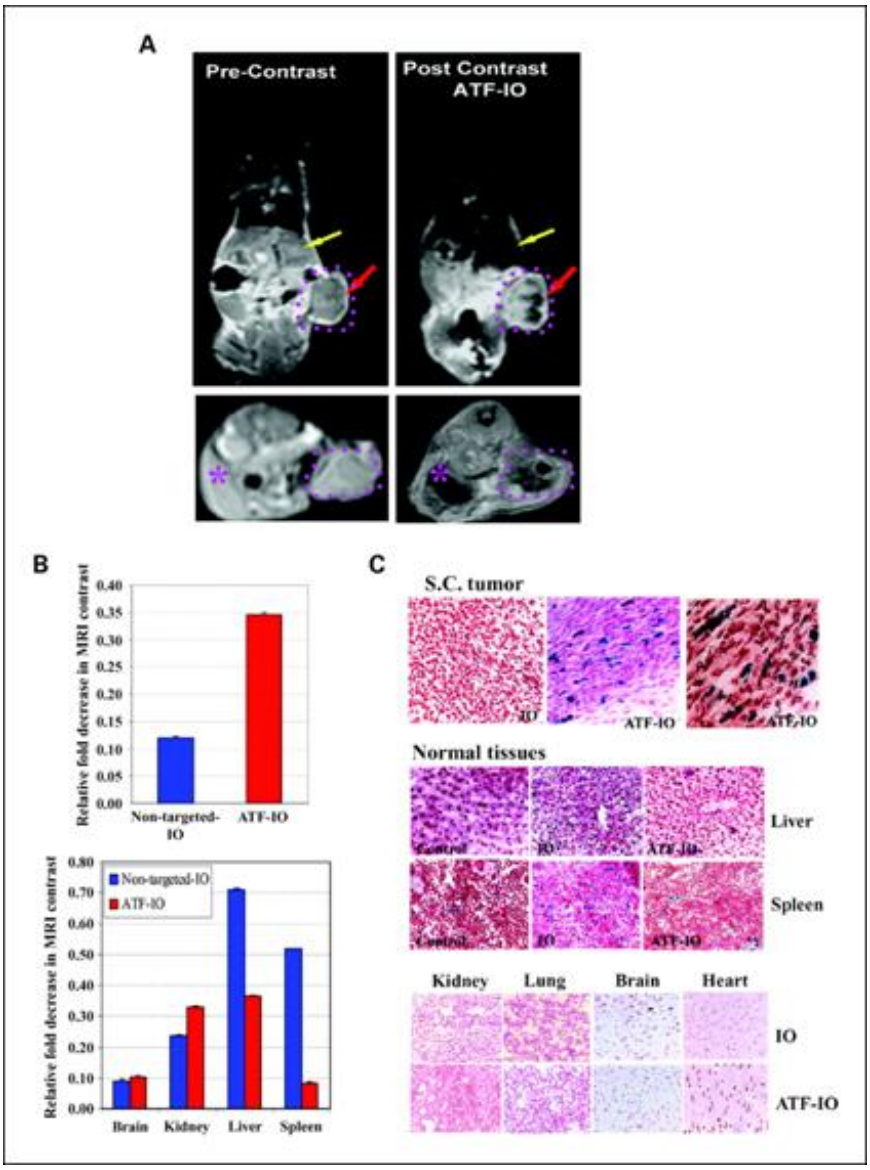

Fig. 2. ***In vivo*** **MRI of 4T1 mammary tumor using ATF-IO nanoparticles.** A, MRI of s.c. mammary tumor. A marked MRI signal drop with T_2 weighted contrast was observed in s.c. tumor areas (pink dashed lined) 6 h after the tail vein injection of ATF-IO nanoparticles. Heterogeneous signal changes suggest that intratumoral distribution of ATF-IO nanoparticles is not uniform in the s.c. tumor (red arrow). T_2 contrast change is also found in the liver (yellow arrows and pink asterisk). Selected MRI image is a representative image of seven mice that received ATF-IO nanoparticles. B, organ-specific profiling of MRI signal change. Signal changes in the mice that received nontargeted iron oxide or ATF-IO nanoparticles for 6 h were measured in the regions of tumor or various normal tissues. Relative intensity was calculated using the intensity in the leg muscle as a reference. Fold decreases in the intensity of MRI were compared between pre– and post–ATF-IO nanoparticle injections and plotted in the figure. Bar plot, mean values of three regions. C, Prussian blue staining of the iron oxide nanoparticles in tumor and normal tissues 48 h after injection of the nanoparticles. Red, background staining with nuclear fast red.

Targeted MRI of i.p. mammary tumor lesions using ATF-IO nanoparticles.
We tested the feasibility of targeting and *in vivo* imaging of metastatic lesions using an animal model bearing i.p. 4T1 tumors. At 5 hours after injection of the ATF-IO nanoparticles, MRI signals decreased in two tumor lesions located on top of the right kidney (Fig. 3, top). The MRI signal in the region recovered gradually 30 hours after the injection of the ATF-IO nanoparticles. In contrast, we did not detect an iron oxide nanoparticle-induced MRI signal change in a tumor-bearing mouse after injection of nontargeted iron oxide (Fig. 3, bottom). The selective accumulation of uPA receptor–targeted ATF-IO nanoparticles in this metastatic i.p. tumor model was further confirmed by Prussian blue staining of tissue sections from the sacrificed animals. A high percentage of iron-positive cells were found in the tumor lesion, whereas the kidney beneath the tumor was negative (Fig. 3, top). On the other hand, we did not detect iron-positive cells in tissue sections of the i.p. tumor mass obtained from the mouse that received nontargeted iron oxide nanoparticles, whereas the adjacent normal liver tissue had a high level of iron-positive cells (Fig. 3, bottom).

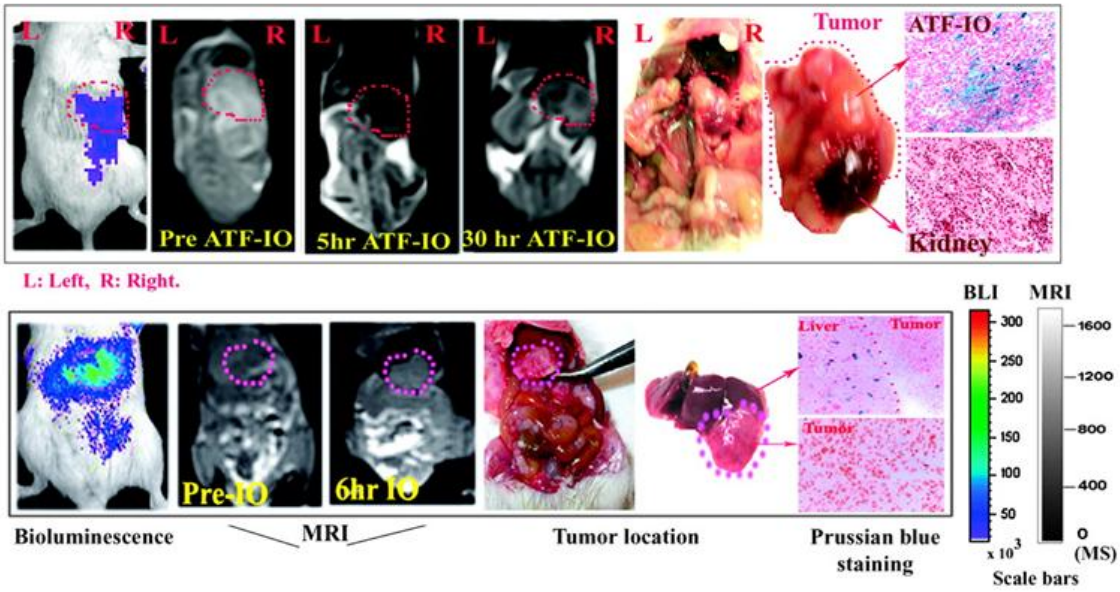

Fig. 3. **Targeting and *in vivo* MRI of i.p. mammary tumor lesions.** Top, bioluminescence imaging detects the presence of i.p. tumors on the upper right of the peritoneal cavity of the mouse. MRI reveal two areas located near the right kidney (red dashed lined) with decreased MRI signals 5 or 30 h after the tail vein injection of 11.2 nmol/kg of body weight of ATF-IO nanoparticles, which corresponded to the locations detected by bioluminescence imaging. Examination of the mouse peritoneal cavity confirmed the locations of two tumor lesions on the top of the right kidney. Specific accumulation of ATF-IO nanoparticles in the tumor tissues was confirmed by Prussian blue staining. Bottom, the control mouse with a tumor lesion in the upper right of the peritoneal cavity received nontargeted iron oxide (IO) nanoparticles. There is no MRI contrast change in the tumor area (pink dashed lined) 6 h after administration of iron oxide nanoparticles, whereas the liver of the mouse shows a marked contrast decrease. Prussian blue staining of tissue sections revealed iron-positive cells in the normal liver near the tumor region but not in the tumor tissues (A red dashed line divides normal liver and tumor tissue areas).